Euro. Jnl of Applied Mathematics (1998), *vol.* 9, *pp.* 561–588. Printed in the United Kingdom

Artificial boundary conditions of absolute transparency for two- and three-dimensional external time-dependent scattering problems

IVAN L. SOFRONOV

Keldysh Institute of Applied Mathematics RAS, Miusskaya sq. 4, Moscow 125047, Russia

(*Received 1 April 1997; revised 21 January 1998*)

For an external problem in $\mathbb{R}^d (d = 2, 3)$ such that the unknown function satisfies the wave equation outside a finite domain, we generate artificial boundary conditions transparent to outgoing waves. These conditions permit an equivalent replacement of the original external problem by the problem inside the artificial boundary which is a circle ($d = 2$) or a sphere ($d = 3$). The questions of numerical implementation of the artificial conditions (that are non-local in both space and time) are considered. Special attention is paid to the reduction of necessary computational resources; in particular, a way of incorporating these conditions into numerical methods which makes the computational formulae local in time is suggested. The aspects of treating artificial boundaries of a non-spherical shape are discussed. Numerical examples of two- and three-dimensional scattering problems demonstrate the accuracy of proposed artificial boundary conditions.

1 Introduction

When numerically simulating physical processes that are connected with the propagation of waves in the whole of space, it is necessary, as a rule, to surround the computational domain by an artificial surface and there impose additional conditions for the unknown functions. Clearly, these Artificial Boundary Conditions (ABC) must be *transparent* for all waves going out to infinity, since the reflected waves will distort a simulation process.

Most known ways for generating ABCs for the wave equation use different *approximate* approaches [1]–[6] (see also the review papers by Givoli [7] and Tsynkov [8]). As a result, the conditions obtained are only transparent for waves with definite frequencies and/or angles of incidence to the artificial boundary.

The ways of generating *exact* ABCs are not so numerous. Ting & Miksis [9] proposed using *Kirchhoff's integral formula* to update the unknown function on the artificial boundary (a numerical investigation of this approach was made by Givoli & Cohen [10]); see also the review by Lyrintzis [11]. The *Fourier method* is used in [12]–[17] to obtain exact ABCs on spherical and circular artificial boundaries: the three-dimensional case is considered in [12]–[17]; the two-dimensional case in [14, 15]. The idea is to write out exact conditions for each Fourier component of the unknown function on the artificial boundary. Notice the approach proposed by Ryaben'kii [18, 19] describing an equivalent

reduction of a *difference* boundary value problem (obtained from an original differential problem) to an appropriate problem in a mesh subdomain.

Exact ABCs are evidently *non-local* in both space and time. Therefore, their numerical implementation can be computationally expensive. Indeed, for each time step, the order of the number of operations required by algorithms based on Kirchhoff's formula is greater so than that required by a simple explicit difference scheme for the wave equation in the computational domain [9]. Nevertheless, this approach is used for practical calculations [20, 21, 11].

At the same time, the conditions proposed by Sofronov and Grote & Keller [12]–[17] are such that the implementation formulae are *local* in time, and therefore they are comparatively cheap. In [12]–[15], the non-local-in-time term of ABCs is represented by convolution operators with respect to time, and special *recurrence formulae* are written out to evaluate these convolutions. Note that similar results in generating effective transparent conditions have been obtained by the author for the problem of transonic flow in wind tunnels [22, 23]. In Grote & Keller [17], local-in-time formulae are obtained by step-by-step solution of auxiliary Cauchy problems for systems of ordinary differential equations on the boundary for each harmonic.

The aim of this paper is to review the results of earlier work [14, 15], and to check our two- and three-dimensional artificial boundary conditions on test problems from Grote & Keller [17] and the *2nd Computational Aeroacoustics Workshop on Benchmark Problems* [24]. In addition, we show that the conditions in Sofronov [12] and Grote & Keller [16] are equivalent.

The outline of the paper is as follows. § 2 presents the formulation of the problem. § 3 and 4 give the theoretical background of the proposed boundary conditions. The questions of their numerical implementation are described in § 5, and § 6 gives the connection between conditions derived in Sofronov [12] and Grote & Keller [16]. The numerical examples are presented in § 7, and we summarise the main issues in § 8.

2 Problem formulation

In $\mathbb{R}^d, d = 2, 3$ we consider a time-dependent problem described by the scalar equation

$$Lv = g \tag{2.1}$$

such that *outside a bounded domain* $D \subset \mathbb{R}^d$

- the function g vanishes;
- the initial data $v|_{t=+0} = v_t|_{t=+0} = 0$;
- the operator L is the wave operator, i.e. $Lv \equiv v_{tt} - c^2 \Delta v$, where $c = const. > 0$ is the propagation speed of waves, Δ is the Laplacian.

The structure of the operator L inside the domain D does not matter for us: L can be any (nonlinear) operator, but we assume that the problem (2.1) has a unique solution.

Equation (2.1) can arise, for example, in problems of acoustic and electromagnetic scattering, fluid dynamics, elasticity, etc., i.e. in those problems where the unknown function satisfies the wave equation outside a given domain.

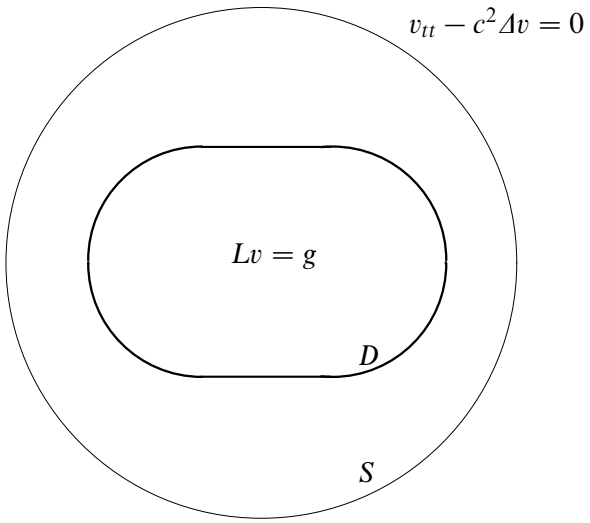

FIGURE 1. Geometry and governing equations of the problem (2.1).

Denote by S a circle (if $d = 2$) or a sphere (if $d = 3$) strictly containing the domain D (see Fig. 1).

Let us consider the following boundary-value problem concurrently with the original one:

$$\begin{cases} L\tilde{v} = g & \text{inside} \quad S \\ \mathscr{T}\tilde{v} = 0 & \text{on} \quad S \end{cases} \tag{2.2}$$

where $\mathscr{T}$ is a linear operator. Our aim is to generate the operator $\mathscr{T}$ so that these two problems are equivalent, i.e. their solutions v and $\tilde{v}$ are identical inside S.

The condition $\mathscr{T}\tilde{v} = 0$ we call the Boundary Condition of Absolute Transparency (BCAT). The word 'absolute' emphasizes the exact character of the conditions.

Note that when using mesh methods for a numerical solution of (2.1), a mesh with a uniform (non-enlarged) spacing in the radial direction must be applied to accurately approximate the waves outgoing to infinity. Therefore, the use of BCAT in numerical methods can reduce computational costs because the size of a computation depends just only on a minimal possible diameter of S.

3 The auxiliary problem

To generate the operator $\mathscr{T}$ in Eq. (2.2), let us consider the following auxiliary problem for the wave equation outside the circle (or sphere if $d = 3$) of radius R:

$$\begin{aligned} &u_{tt} - c^2 \Delta u = 0, && r > R, \quad t > 0 \\ &u|_{t=+0} = u_t|_{t=+0} = 0, && r > R \\ &u|_{r=R} = f(t); \end{aligned} \tag{3.1}$$

$f(t)$ is a given function, $c = const > 0$.

We solve this problem by using the Fourier method. Let us expand u in harmonics $e^{im\phi}$

https://doi.org/10.1017/S0956792598003507 Published online by Cambridge University Press

if $d = 2$:

$$u(r, \phi, t) = \sum_{m=-\infty}^{\infty} v_m(r, t) e^{im\phi}, \tag{3.2}$$

or in spherical functions $Y_l^m(\theta, \phi) = P_l^{|m|}(\cos\theta) e^{im\phi}$ if $d = 3$:

$$u(r, \theta, \phi, t) = \sum_{l=0}^{\infty} \sum_{m=-l}^{l} v_l^m(r, t) Y_l^m(\theta, \phi). \tag{3.3}$$

The function f is also represented by Fourier coefficients f_m if $d = 2$, or by f_l^m if $d = 3$. Substituting Eq. (3.2) (or (3.3)) for the problem (3.1), we see that each function $w \equiv v_m$ (or $w \equiv v_l^m$) must be a solution of the problem

$$\begin{aligned} &w_{tt} - \frac{c^2}{r^{d-1}}(r^{d-1} w_r)_r + \frac{c^2}{r^2}\lambda_\nu w = 0, && r > R,\ t > 0 \\ &w|_{t=+0} = w_t|_{t=+0} = 0, && r > R \\ &w|_{r=R} = \hat{f}(t), \end{aligned} \tag{3.4}$$

where $\lambda_\nu = \nu^2$, $\nu = |m|$, $\hat{f} = f_m$ in the case $d = 2$; and $\lambda_\nu = \nu^2 - \frac{1}{4}$, $\nu = l + \frac{1}{2}$, $\hat{f} = f_l^m$ in the case $d = 3$.

Let us represent the solution of Eq. (3.4) by the convolution $w(r, t) = \hat{f}(t) * G_\nu(r, t)$ where $G_\nu(r, t)$ is the Green's function of the following problem

$$\begin{aligned} &L_\nu G_\nu = 0, && r > R,\ t > 0 \\ &G_\nu|_{t=+0} = \frac{\partial}{\partial t} G_\nu|_{t=+0} = 0, && r > R \\ &G_\nu|_{r=R} = \delta(t). \end{aligned} \tag{3.5}$$

Here L_ν is the differential operator of the problem (3.4) and $\delta(t)$ is the Dirac delta-function.

To find G_ν let us use the Laplace transform technique. We write

$$g_\nu(r, p) = \mathscr{L}[G_\nu](r, p) \equiv \int_0^\infty G_\nu(r, t) e^{-pt} dt,$$

the transform of G_ν. Then the following problem arises for g_ν:

$$\begin{aligned} &\frac{1}{r^{d-1}} \frac{d}{dr}\left(r^{d-1} \frac{d}{dr} g_\nu\right) - \left(\frac{p^2}{c^2} + \frac{\lambda_\nu}{r^2}\right) g_\nu = 0, && r > R \\ &g_\nu|_{r=R} = 1, \quad g_\nu|_{r\to\infty} = 0. \end{aligned} \tag{3.6}$$

The solution of this problem is written by using Macdonald's cylindrical functions $\mathrm{K}_\nu(z)$ and has the form

$$g_\nu(r, p) = \left(\frac{R}{r}\right)^{\frac{d-2}{2}} \frac{\mathrm{K}_\nu(pr/c)}{\mathrm{K}_\nu(pR/c)}.$$

Expressing $\mathrm{K}_\nu(z)$ in terms of Tricomi's confluent hypergeometric function $\Psi(\nu + \frac{1}{2}, 2\nu + 1; 2z)$, we have

$$\begin{aligned} g_\nu(r, p) &= \left(\frac{R}{r}\right)^{-\nu + \frac{d-2}{2}} \exp\left(-p\frac{r - R}{c}\right) \frac{\Psi(\nu + \frac{1}{2}, 2\nu + 1; \frac{2rp}{c})}{\Psi(\nu + \frac{1}{2}, 2\nu + 1; \frac{2Rp}{c})} \\ &= \left(\frac{R}{r}\right)^{\frac{d-1}{2}} \exp\left(-p\frac{r - R}{c}\right) + \left(\frac{R}{r}\right)^{\frac{d-2}{2}} \exp\left(-p\frac{r - R}{c}\right) \psi_\nu(r, p), \end{aligned}$$

https://doi.org/10.1017/S0956792598003507 Published online by Cambridge University Press

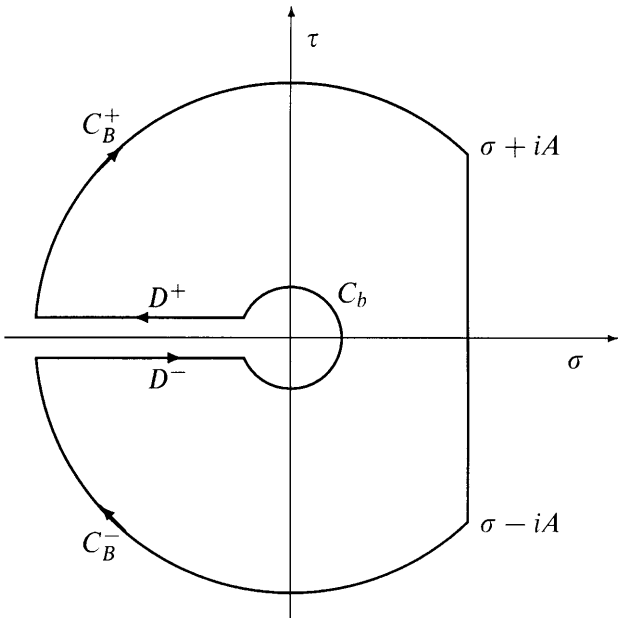

FIGURE 2. The contour of integration.

where

$$\psi_\nu(r,p) \equiv \left(\frac{R}{r}\right)^{-\nu} \frac{\Psi(\nu+\frac{1}{2}, 2\nu+1; \frac{2rp}{c})}{\Psi(\nu+\frac{1}{2}, 2\nu+1; \frac{2Rp}{c})} - \left(\frac{R}{r}\right)^{\frac{1}{2}}.$$

To find $G_\nu(r,t)$ we have to apply the inverse Laplace transform to $g_\nu(r,p)$, i.e. to calculate the integral

$$G_\nu(r,t) = \frac{1}{2\pi i} \int_{\sigma-i\infty}^{\sigma+i\infty} e^{pt} g_\nu(r,p) dp.$$

Substituting the expression of $g_\nu(r,p)$ for this integral and using well-known properties of the Laplace transform, we have

$$G_\nu(r,t) = \left(\frac{R}{r}\right)^{\frac{d-1}{2}} \delta\left(t - \frac{r-R}{c}\right) + \left(\frac{R}{r}\right)^{\frac{d-2}{2}} \theta\left(t - \frac{r-R}{c}\right) F_\nu\left(r, t - \frac{r-R}{c}\right) \tag{3.7}$$

where

$$F_\nu(r,t) = \frac{1}{2\pi i} \int_{\sigma-i\infty}^{\sigma+i\infty} e^{pt} \psi_\nu(r,p) dp;$$

$\theta(t)$ denotes the Heaviside function. We use contour integration [25] to calculate the integral $F_\nu(r,t)$, and consider a contour consisting of: *(a)* the segment $[\sigma - iA, \sigma + iA]$; *(b)* the arcs C_B^+ and C_B^- of the circle $|p| = B$; *(c)* the double-sided cut D^+, D^-; and *(d)* the circle C_b, $|p| = b$ – see Fig. 2 (the direction of integration is pointed by arrows).

Because of the asymptotic properties of $\Psi(\nu+\frac{1}{2}, 2\nu+1; 2z)$, function $\psi_\nu(r,p)$ converges uniformly to zero as $|p| \to \infty$. Applying Jordan's lemma, we see that the integrals along

https://doi.org/10.1017/S0956792598003507 Published online by Cambridge University Press

the arcs C_B^+ and C_B^- go to zero as $B \to \infty$. The integral along the arc C_B also vanishes as $b \to 0$ since $\psi_v(r,p)$ is bounded as $|p| \to 0$. Taking $p = -s \pm i0, s \geqslant 0$ let us write the integrals along the cut D^+, D^- in the form

$$I_v^{\pm} = \mp \frac{1}{2\pi i} \int_0^{\infty} \mathrm{e}^{-st} \psi_v(r, -s \pm i0) ds.$$

Using the residue theorem, we have

$$F_v(r,t) = I_v^+(r,t) + I_v^-(r,t) + \sum_{j=1}^{J} \mathrm{e}^{p_j t} \mathrm{Res} \psi_v(r, p_j), \tag{3.8}$$

where p_j are the poles of $\psi_v(r,p)$.

3.1 Two-dimensional case

Let us first consider the case $d = 2$. Here $v = |m|$.

By using the specific expression for $\Psi(|m| + \frac{1}{2}, 2|m| + 1; z)$ at integer $|m|$ [26], we obtain that the sum of integrals along the cut can be written in the form

$$I_v^+(r,t) + I_v^-(r,t) = -\frac{1}{\pi} \left(\frac{r}{R}\right)^{|m|} \int_0^{\infty} \mathrm{e}^{-st} \mathrm{Im} \frac{\Psi(|m| + \frac{1}{2}, 2|m| + 1; \frac{-2r}{c} s + i0)}{\Psi(|m| + \frac{1}{2}, 2|m| + 1; \frac{-2R}{c} s + i0)} ds$$

$$= -\frac{1}{\pi} \frac{c}{2R} \left(\frac{r}{R}\right)^{|m|} \int_0^{\infty} \exp\left(-\frac{c}{2R} st\right) h_{|m|}(r,s) ds, \tag{3.9}$$

where

$$h_{|m|}(r,s) = \mathrm{Im} \frac{\Psi(|m| + \frac{1}{2}, 2|m| + 1; -\frac{r}{R} s + i0)}{\Psi(|m| + \frac{1}{2}, 2|m| + 1; -s + i0)} \tag{3.10}$$

and Imz denotes the imaginary part of z.

It is most likely that the latter integral (which is the Laplace transform of $h_{|m|}$) does not have an explicit quadrature. Therefore, we calculate it numerically when implementing the condition of absolute transparency – see § 5. The following asymptotic property of $h_{|m|}(r,s)$ makes this procedure computationally cheap.

Lemma *The function $h_{|m|}(r,s)$ converges to $C_r \mathrm{e}^{-s}$ as $s \to \infty$, where C_r is a constant depending on r.*

Proof By using formulae relating $\Psi(|m| + \frac{1}{2}, 2v + 1; z)$ and Kummer's confluent hypergeometric function $\Phi(|m| + \frac{1}{2}, 2v + 1; z)$ [26], we have

$$\Psi\left(|m| + \frac{1}{2}, 2|m| + 1; -s + i0\right)$$

$$= \mathrm{e}^{-s} \left[\Psi\left(|m| + \frac{1}{2}, 2|m| + 1; s\right) + \frac{\sqrt{\pi}(-1)^{|m|+1}}{4^{|m|} |m|!} \Phi\left(|m| + \frac{1}{2}, 2|m| + 1; s\right) i \right].$$

https://doi.org/10.1017/S0956792598003507 Published online by Cambridge University Press

Because of the well-known asymptotic properties

$$\Psi\left(|m|+\frac{1}{2},2|m|+1;s\right)\sim s^{-\left(|m|+\frac{1}{2}\right)}$$

and

$$\Phi\left(|m|+\frac{1}{2},2|m|+1;s\right)\sim\left(\frac{\sqrt{\pi}}{4^{|m|}|m|!}\right)^{-1}\mathrm{e}^{s}s^{-\left(|m|+\frac{1}{2}\right)}$$

as $s\to\infty$, we have

$$h_{|m|}(r,s)\sim\left(\frac{r}{R}\right)^{-\left(|m|+\frac{1}{2}\right)}\mathrm{Im}\frac{\mathrm{e}^{-rs/R}+(-1)^{|m|+1}i}{\mathrm{e}^{-s}+(-1)^{|m|+1}i}$$

$$=\left(\frac{r}{R}\right)^{-\left(|m|+\frac{1}{2}\right)}(-1)^{|m|+1}\mathrm{e}^{-s}(1+o(1)).$$

This formula proves our lemma with $C_r=(-1)^{|m|+1}\left(\frac{r}{R}\right)^{-\left(|m|+\frac{1}{2}\right)}$. □

Denote by $z_j^{|m|}$, $j=1,2,...,J$, the roots of the Tricomi's function $\Psi(|m|+\frac{1}{2},2|m|+1;z)$. From the relationship $\mathrm{K}_\nu(z)=\sqrt{\pi}(2z)^\nu\mathrm{e}^{-z}\Psi(\nu+\frac{1}{2},2\nu+1;2z)$, we see that the values $0.5z_j^{|m|}$ are the roots of the Macdonald's function. It is known [27] for $\nu=|m|$ that the roots of the Macdonald's function are simple and complex conjugate. Their number $J=|m|$ if $|m|$ is even, and $J=|m|-1$ otherwise, i.e. $J=2\left[\frac{|m|}{2}\right]$, where $[a]$ denotes the entire part of a. Therefore, by using the formula for the residue in the case of a simple pole, and substituting $p_j=cz_j^{|m|}/(2R)$, we rewrite the third term of (3.8) by

$$\sum_{j=1}^{J}\mathrm{e}^{p_jt}\mathrm{Res}\psi_\nu(r,p_j)=\frac{c}{2R}\left(\frac{r}{R}\right)^{|m|}\sum_{j=1}^{2\left[\frac{|m|}{2}\right]}\mathrm{e}^{\frac{cz_j^{|m|}}{2R}t}\frac{\Psi(|m|+\frac{1}{2},2|m|+1;\frac{r}{R}z_j^{|m|})}{\Psi'(|m|+\frac{1}{2},2|m|+1;z_j^{|m|})},\tag{3.11}$$

where Ψ' denotes the derivative of Ψ with respect to the argument.

Substituting (3.8), (3.9) and (3.11) for (3.7) and convolving the Green's function $G_\nu(r,t)$ with $\hat{f}(t)$, we obtain the following solution of the problem (3.4) for the two-dimensional case:

$$\begin{aligned}w(r,t)=&\left(\frac{R}{r}\right)^{1/2}\hat{f}\left(t-\frac{r-R}{c}\right)\\&+\frac{c}{2R}\left(\frac{r}{R}\right)^{|m|}\int_0^{t-\frac{r-R}{c}}\hat{f}(t')\left\{-\frac{1}{\pi}\int_0^\infty\exp\left(-s\left(t-\frac{r-R}{c}-t'\right)\right)h_{|m|}(r,s)ds\right\}dt'\\&+\frac{c}{2R}\left(\frac{r}{R}\right)^{|m|}\int_0^{t-\frac{r-R}{c}}\hat{f}(t')\left\{\sum_{j=1}^{2\left[\frac{|m|}{2}\right]}\exp\left(\frac{cz_j^{|m|}}{2R}\left(t-\frac{r-R}{c}-t'\right)\right)a_j^{|m|}(r)\right\}dt'.\end{aligned}\tag{3.12}$$

Here $h_{|m|}(r,s)$ is defined by (3.10);

$$a_j^{|m|}(r)\equiv\frac{\Psi(|m|+\frac{1}{2},2|m|+1;\frac{r}{R}z_j^{|m|})}{\Psi'(|m|+\frac{1}{2},2|m|+1;z_j^{|m|})};$$

https://doi.org/10.1017/S0956792598003507 Published online by Cambridge University Press

$z_j^{|m|}$ are the roots of $\Psi(|m| + \frac{1}{2}, 2|m| + 1; z)$; the third term is omitted if $|m| = 0$ or $|m| = 1$.

3.2 Three-dimensional case

Consider now the case $d = 3$. Here $\nu = l + \frac{1}{2}$. For $\nu = l + \frac{1}{2}$, the confluent hypergeometric function is expressed in the terms of the Laguerre polynomial $L_n^{(\alpha)}(z)$ [26], and has the form

$$\Psi(l + 1, 2l + 2; z) = \frac{(2l)!}{l!} z^{-(2l+1)} L_l^{(-2l-1)}(z).$$

Therefore, the function $\psi_\nu(r, p)$ is univalent, and the integrals along the cut D^+, D^- are mutually annihilated.

As a result, only the third term remains in Eq. (3.8). Transforming this term in a similar way as was done for the two-dimensional case, and convolving Green's function (3.7) with $\hat{f}$, we find the following formula for the solution of the problem (3.4) in the three-dimensional case:

$$w(r,t) = \frac{R}{r}\hat{f}\left(t - \frac{r-R}{c}\right) + \frac{c}{2R}\left(\frac{R}{r}\right)^{l+1} \int_0^{t-\frac{r-R}{c}} \hat{f}(t') \left\{ \sum_{j=1}^{l} \exp\left(\frac{cz_j^l}{2R}\left(t - \frac{r-R}{c} - t'\right)\right) a_j^l(r) \right\} dt'. \tag{3.13}$$

Here

$$a_j^l(r) = \frac{L_l^{(-2l-1)}\left(\frac{r}{R} z_j^l\right)}{\left(L_l^{(-2l-1)}\left(z_j^l\right)\right)'}$$

(the prime denotes the derivative with respect to the argument); z_j^l are the roots of Laguerre polynomial $L_l^{(-2l-1)}(z)$; the second term is omitted if $l = 0$.

By substituting Eq. (3.12) with $w \equiv v_m$, $\hat{f} \equiv f_m$ and (3.13) with $w \equiv v_l^m$, $\hat{f} \equiv f_l^m$ for the series (3.2) and (3.3), respectively, we obtain the formal solution of the auxiliary problem (3.1).

4 Conditions of absolute transparency

Denote by Q the operation of Fourier expansion of an arbitrary function defined on the circle ($d = 2$) or on the sphere ($d = 3$) in the series (3.2) or (3.3), respectively, i.e. Q is the operator generating the set of Fourier coefficients according to the following formulae:

$$v_m(r,t) = \frac{1}{2\pi} \int_0^{2\pi} u(r, \phi, t) \mathrm{e}^{-im\phi} d\phi, \quad \text{for} \quad d = 2 \tag{4.1}$$

and

$$v_l^m(r,t) = \frac{2l+1}{4\pi} \frac{(l-m)!}{(l+m)!} \int_0^{2\pi} \int_0^{\pi} u(r, \theta, \phi, t) Y_l^m(\theta, \phi) \sin\theta d\theta d\phi, \quad \text{for} \quad d = 3. \tag{4.2}$$

https://doi.org/10.1017/S0956792598003507 Published online by Cambridge University Press

We denote by Q^{-1} the inverse operator, i.e. the operator of summation according to Eq. (3.2) or Eq. (3.3).

Let us write the operator $\mathscr{T}$ for $d = 2$ in the form of

$$\mathscr{T} = Q^{-1}\{\mathscr{T}_m\}Q, \tag{4.3}$$

and for $d = 3$ in the form of

$$\mathscr{T} = Q^{-1}\{\mathscr{T}_l^m\}Q, \tag{4.4}$$

and define the operators $\{\mathscr{T}_m\}$ and $\{\mathscr{T}_l^m\}$ as block-diagonal ones with block operators $\mathscr{T}_m$ for $d = 2$ and $\mathscr{T}_l^m$ for $d = 3$ acting independently on each Fourier coefficient with the index (m) and multi-index $\binom{m}{l}$, respectively.

Let us consider first the case $d = 2$. The formula (3.12) gives the solution of the Dirichlet problem (3.4) with $\hat{f} = w|_{r=R}$. Denoting $\varepsilon = r - R$, we have from Eq. (3.12):

$$\frac{1}{\varepsilon}\left(w(R+\varepsilon,t) - \sqrt{\frac{R}{R+c}}\,w\left(R, t-\frac{\varepsilon}{c}\right)\right)$$

$$= \frac{c}{2R}\left(\frac{R+\varepsilon}{R}\right)^{|m|}\int_0^{t-\frac{\varepsilon}{c}} w(R,t')\left\{-\frac{1}{\pi}\int_0^{\infty}\exp\left(-s\left(t-\frac{\varepsilon}{c}-t'\right)\right)\frac{1}{\varepsilon}h_{|m|}(R+\varepsilon,s)ds\right.$$
$$\left. + \sum_{j=1}^{2\left[\frac{|m|}{2}\right]}\exp\left(\frac{cz_j^{|m|}}{2R}\left(t-\frac{\varepsilon}{c}-t'\right)\right)\frac{1}{\varepsilon}a_j^{|m|}(r)\right\}dt'.$$

Taking the limit as $\varepsilon \to +0$, we find

$$\mathscr{T}_m w = 0 \tag{4.5}$$

with the operator $\mathscr{T}_m$ defined by

$$\mathscr{T}_m w \equiv \frac{\partial}{\partial t}w + \frac{c}{\sqrt{r}}\frac{\partial}{\partial r}(\sqrt{r}w) - \int_0^t E_m^{(2)}(r,t-t')w(r,t')dt',$$

where the kernel of the convolution has the form

$$E_m^{(2)}(r,t) = \frac{c^2}{2r^2}\left\{(-1)^{|m|}\int_0^{\infty}\frac{e^{-st}ds}{\pi^2 I_m^2(s/2) + K_m^2(s/2)} + \sum_{j=1}^{2\left[\frac{|m|}{2}\right]} e^{\frac{cz_j^{|m|}}{2r}t}z_j^{|m|}\right\};$$

the last term in $E_m^{(2)}(r,t)$ is omitted if $|m| = 0$ or $|m| = 1$. Here $I_m(s)$ is the Bessel function of an imaginary argument, and $K_m(s)$ is Macdonald's function. The formulae for evaluating the limit of the term $\frac{1}{\varepsilon}h_{|m|}(R+\varepsilon,s)$ are given in the Appendix.

Treating the three-dimensional case ($d = 3$) in a similar way, we obtain that Eq. (3.13) yields the equality

$$\mathscr{T}_l^m w = 0, \tag{4.6}$$

https://doi.org/10.1017/S0956792598003507 Published online by Cambridge University Press

where

$$\mathscr{T}_l^m w \equiv \frac{\partial}{\partial t} w + \frac{c}{r}\frac{\partial}{\partial r}(rw) - \int_0^t E_l^{(3)}(r, t-t')w(r,t')dt', \tag{4.7}$$

$$E_l^{(3)}(r,t) = \frac{c^2}{2r^2}\sum_{j=1}^{l} \exp\left(\frac{cz_j^l}{2r}\, t\right) z_j^l,$$

the function $E_l^{(3)}(r,t) = 0$ if $l = 0$. Note that $\mathscr{T}_l^m$ does not depend on the superscript m.

According to Watson [27], the roots of $K_\nu(z)$, $\nu > 0$, have negative real parts which implies the stability of the evaluation of convolution operators in Eqs. (4.5) and (4.6) while numerical implementing BCAT.

Having generated the operator $\mathscr{T}$ in this way, we formulate the following theorem about the equivalence of problems (2.1) and (2.2).

Theorem 1. *The solution v of the problem* (2.1) *is also the solution of the problem* (2.2)*;*
2. *Let $\tilde{v}$ be a solution of the problem* (2.2) *and $\tilde{v} = \tilde{v}_t = 0$ at $r > R$, $t = 0$. Suppose also that this function is twice-differentiable up to S. Then $\tilde{v}$ can be extended outside S to a solution of the problem* (2.1).

Proof In the first part of the theorem we have to prove only that $\mathscr{T} v = 0$ on S, since the governing equation is the same for both problems inside S. This equality follows immediately from the way of constructing $\mathscr{T}$ taking account that v is the solution of the auxiliary problem (3.1) due to conditions (1)–(3) of problem (2.1).

Let us prove the second part of the theorem. Take $f = \tilde{v}|_S$ in problem (3.1). Then Eqs. (3.2), (3.12) (or (3.3), (3.13)) give v satisfying the statement of the theorem for $r > R$. Considering now v as the definition of $\tilde{v}$ outside S, we denote the whole of this function by $\tilde{v}$. According to the construction, $\tilde{v}$ is continuous at $r = R$ and satisfies the wave equation at $r = R - 0$ and at $r > R$. It remains to prove that it also satisfies the wave equation at $r = R$.

Since Eq. (4.5) (or (4.6)) is the corollary of Eq. (3.12) (or (3.13)), then $\mathscr{T}\tilde{v} = 0$ at $r = R + 0$. Using the theorem condition $\mathscr{T}\tilde{v} = 0$ at $r = R - 0$, and the continuity of $\tilde{v}$, we have $\frac{\partial \tilde{v}}{\partial r}|_{R-0} = \frac{\partial \tilde{v}}{\partial r}|_{R+0}$, i.e. $\tilde{v}$ has continuous derivatives at $r = R$. Let us write the wave equation in polar (if $d = 2$) or spherical (if $d = 3$) coordinates. From the fact that continuously-differentiable function $\tilde{v}$ satisfies this equation from the right and from the left of the point $r = R$, we obtain $\frac{\partial^2 \tilde{v}}{\partial r^2}|_{R-0} = \frac{\partial^2 \tilde{v}}{\partial r^2}|_{R+0}$. Thus, $\tilde{v}$ has continuous derivatives at least up to the second order at $r = R$ and it satisfies the wave equation for $r = R - 0$ and $r > R$; therefore it satisfies the wave equation also at $r = R$. □

5 Application of conditions of absolute transparency in numerical methods

It is clear that a straightforward use of the operators (4.3), (4.4) is only possible in the case of spherical meshes near the external boundary of a computational domain. Moreover, different numerical schemes for the governing equation inside the computational domain

https://doi.org/10.1017/S0956792598003507 Published online by Cambridge University Press

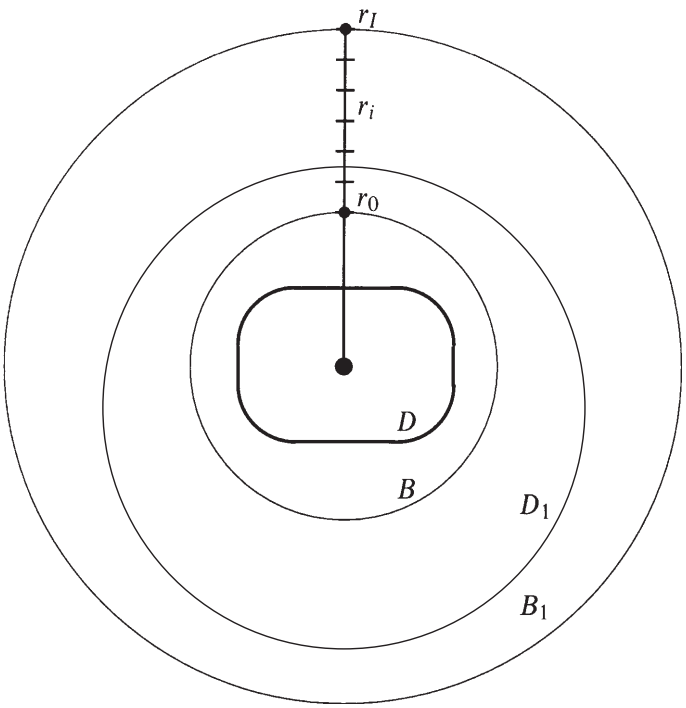

FIGURE 3. The location of domains.

(explicit or implicit ones) can influence the discretization of (4.3), (4.4). Therefore, we propose another approach to generate the desired numerical conditions. The idea is to use the representation formulae (3.12), (3.13) to calculate the solution on the external boundary in terms of the solution inside the computational domain. Such an approach does not depend on the method of evaluating the solution in D, and permits us to treat both spherical and non-spherical meshes: as we will see, the difference consists only of an additional interpolation procedure for the last case. Note that, although discretization of (3.12), (3.13) can be made with any desired accuracy, it makes no sense to take it higher than the accuracy of the numerical method used inside the computational domain; in what follows, we describe the approximation having the second-order discretization error.

For the problem (2.1), let us consider an auxiliary domain D_1 and d-dimensional ball B of a radius R (see Fig. 3) such that the following three assumptions are valid:

(1) $D \subseteq B \subset D_1$;

(2) we have a numerical method of step-by-step time integration of equation (2.1) in the domain D_1 with the Dirichlet condition $v = v_b$ on the boundary of D_1 (here v_b is a given function);

(3) the distance between the surfaces of B and D_1 is greater than the value $c\tau_{max}$, where τ_{max} is the maximal time step achieved in the process of numerical solution of the problem in the domain D_1.

https://doi.org/10.1017/S0956792598003507 Published online by Cambridge University Press

Let M_D be a mesh in the domain D_1 for the proposed numerical method. Denote by v^n the solution on the nth time level, i.e. at $t = t_n$. Our aim is to calculate the value v_b on the $(n+1)$st time level in terms of v^n by using the explicit formulae for the solution of the auxiliary problem (3.1).

We subdivide this calculation into three stages described below. § 5.1 contains the formulae for the three-dimensional case. The two-dimensional case is considered in § 5.2. In § 5.3, we discuss the necessary computational resources for the case of spherically-shaped artificial boundaries.

5.1 Three-dimensional case

Stage 1

Let B_1 be a ball of radius R_1 with the same centre as B such that $D_1 \subseteq B_1$. Introduce a spherical mesh between the surfaces of B and B_1:

$$\begin{aligned} r_i &= R + ih_r,\ h_r = (R_1 - R)/I,\ i = 0, 1, ..., I; \\ \theta_j &= (j + \tfrac{1}{2})h_\theta, \quad h_\theta = \pi/J, \quad j = 0, 1, ..., J-1; \\ \phi_k &= kh_\phi, \quad h_\phi = 2\pi/K, \quad k = 0, 1, ..., K-1, \end{aligned} \tag{5.1}$$

where I, J, K are natural numbers.

To approximate the operators Q and Q^{-1} (see (4.2) and (3.3)), we use the Difference Spherical Functions (DSF) technique introduced by Ryaben'kii & Sofronov [28] (see also [29]). These DSFs are the eigenfunctions of a central-difference counterpart of the Beltrami operator on the mesh $\{\theta_j, \phi_k\}$ and they form an orthonormal basis of dimension $J \times K$. Each DSF with fixed indexes converges to the appropriate spherical function as the mesh parameters J and K increase. Efficient numerical procedures for calculating and exploring *DSFs* are proposed in Ryaben'kii & Sofronov [28].

Let us fix a number L, $L \leqslant J \leqslant K/2$, and consider the subspace of difference spherical functions $\{Y_{JK}^{l,m}(\theta_j, \phi_k)\}$ with the set of indexes $\mathscr{M} = \{l = 0, 1, ..., L; m = -l, ..., l\}$.

At this stage, we first interpolate the discrete function v^n from the mesh M_D onto the spherical mesh $\{\theta_j, \phi_k\}$ at $r = R$ and obtain a function $v^n(\theta_j, \phi_k)$. Then we expand $v^n(\theta_j, \phi_k)$ in *DSFs*:

$$c_l^m = \sum_{j=0}^{J} \sum_{k=0}^{K} Y_{JK}^{l,m}(\theta_j, \phi_k) v^n(\theta_j, \phi_k) \sin\theta_j \, h_\theta \, h_\phi.$$

As a result, we have the set of coefficients denoted by $\{c_l^m(R, t_n)\}$, $\binom{m}{l} \in \mathscr{M}$; the coefficient $c_l^m(R, t_n)$ corresponds to the spherical function Y_l^m.

Stage 2

Denote by I_0 a value of i such that r_{I_0} is the maximal radius of a sphere belonging strictly to the domain D_1. In the second stage, we calculate $c_l^m(r, t)$ for each $\binom{m}{l} \in \mathscr{M}$ in the points $r = r_{I_0}, r_{I_0+1}, \cdots, r_I$, $t = t_{n+1}$ on the basis of its values at $r = R$, $t = 0, t_1, \cdots, t_n$.

Let $H_i = ih_r$, $i = I_0, \cdots, I$. Denote by $\kappa \geqslant 0$ an integer such that $t_{n-\kappa-1} + H_i/c < t_{n+1} \leqslant$

https://doi.org/10.1017/S0956792598003507 Published online by Cambridge University Press

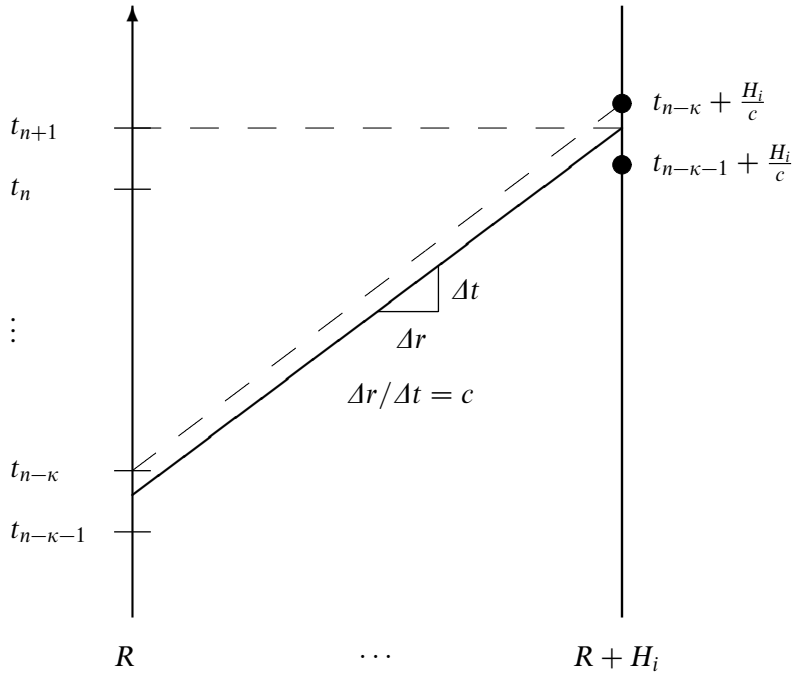

FIGURE 4. Calculation of $c_l^m(R+H_i, t_{n-\kappa}+H_i/c)$.

$t_{n-\kappa}+H_i/c$ (see Fig. 4). Assumption 3 for the domain D_1 and the ball B ensures the existence of such a κ.

Calculate first the value $c_l^m(R+H_i, t_{n-\kappa}+H_i/c)$. Since the function $c_l^m(r,t)$ must satisfy problem (3.4) with $\hat{f}(t) \equiv c_l^m(R,t)$, we use (3.13) to represent the solution. Rearranging the operations of summation and integration in (3.13), we obtain

$$c_l^m(R+H_i, t_{n-\kappa}+H_i/c) = \frac{R}{R+H_i} c_l^m(R, t_{n-\kappa}) + \sum_{j=1}^{l} d_j^l(H_i) q_j^l(t_{n-\kappa}),$$

where

$$d_j^l(H_i) = \frac{c}{2R}\left(\frac{R}{R+H_i}\right)^{l+1} \frac{L_l^{(-2l-1)}\left(\frac{R+H_i}{R} z_j^l\right)}{\left(L_l^{(-2l-1)}\left(z_j^l\right)\right)'},$$

$$q_j^l(t_{n-\kappa}) = q_j^l(t_{n-\kappa-1}) \exp\left(\alpha_j^l \tau_{n-\kappa}\right) + s_j^l(t_{n-\kappa}), \qquad q_j^l(0) = 0, \tag{5.2}$$

$$\tau_{n-\kappa} = t_{n-\kappa} - t_{n-\kappa-1}, \quad \alpha_j^l = c z_j^l/(2R),$$

$$s_j^l(t_{n-\kappa}) = \int_{t_{n-\kappa-1}}^{t_{n-\kappa}} c_l^m(R,t) \exp[\alpha_j^l(t_{n-\kappa}-t)]\,dt.$$

Recall that no calculations of d_j^l, q_j^l are required for $l = 0$.

https://doi.org/10.1017/S0956792598003507 Published online by Cambridge University Press

To calculate the values $s_j^l(t_{n-\kappa})$, it is necessary to interpolate the discrete function $c_l^m(R,t)$ on the interval $(t_{n-\kappa-1}, t_{n-\kappa})$ by using its values at the points $t = 0, t_1, \cdots, t_n$. We use here the simple linear interpolation. Therefore, we have

$$s_j^l(t_{n-\kappa}) = c_l^m(R, t_{n-\kappa})\frac{e^{\alpha_j^l \tau_{n-\kappa}} - 1}{\alpha_j^l}$$

$$+[c_l^m(R, t_{n-\kappa}) - c_l^m(R, t_{n-\kappa-1})]\frac{(1 - \alpha_j^l \tau_{n-\kappa})e^{\alpha_j^l \tau_{n-\kappa}} - 1}{(\alpha_j^l)^2 \tau_{n-\kappa}}.$$

The values $c_l^m(R + H_i, t_{n-\kappa-1} + H_i/c)$ are calculated in the same way.

Finally, we obtain the desired value $c_l^m(R + H_i, t_{n+1})$ by the linear interpolation of $c_l^m(R + H_i, t_{n-\kappa} + H_i/c)$ and $c_l^m(R + H_i, t_{n-\kappa-1} + H_i/c)$.

The evaluations described in this stage are made for all indexes $\binom{m}{l} \in \mathscr{M}$.

Note that the recurrence relations (5.2) are used to calculate the values of $q_j^l(t_{n-\kappa})$. Moreover, the values $q_j^l(t_{n-\kappa})$ and $s_j^l(t_{n-\kappa})$ do not depend on the parameter H_i.

Thus although the operator $\mathscr{T}$ is non-local in time, the proposed implementation of the discrete formulae is *local* in time due to the recurrence relations for the functions $q_j^l(t_{n-\kappa})$. This remarkable property is corollary of the fact that the kernels $E_l^{(3)}(r,t)$ of convolutions in $\mathscr{T}$ are finite sums of exponentials.

Remark. Linear interpolation has been used for calculating $s_j^l(t_{n-\kappa})$ and $c_l^m(R + H_i, t_{n+1})$. It gives an error $\mathcal{O}(\tau^2)$. To get a higher accuracy, one may apply here a quadratic or cubic interpolation by using the points at $t = t_{n-\kappa-2}$ or at $t = t_{n-\kappa-2}$, $t_{n-\kappa-3}$, respectively. In our test calculations, quadratic interpolation is used.

Stage 3

In the final stage, we calculate finite series on DSFs (difference counterparts of (3.3), $l = 0, 1, ..., L$) with coefficients $c_l^m(r_i, t_{n+1})$, $\binom{m}{l} \in \mathscr{M}$ obtained for each sphere $r = r_i$, i.e. we calculate

$$v_b(r_i, \theta_j, \phi_k) = \sum_{l,m \in \mathscr{M}} c_l^m(r_i, t_{n+1}) Y_{JK}^{l,m}(\theta_j, \phi_k), \quad i = I_0, \cdots, I.$$

Thus we have the values of v_b on the mesh $\{r_i, \theta_j, \phi_k\}$. By interpolating these values into points $\{r, \theta, \phi\}$ of the mesh M_D belonging to the surface of D_1, we find the updated function v_b.

Remark. To reduce computational costs, it is preferable to generate a mesh $\{r_i\}$ using the set of Chebyshev nodes instead of the simplest uniform mesh (5.1).

Note that minimal computational costs for implementing BCAT are achieved if $D_1 = B_1$, and the surface of B is one of the coordinate surfaces of the mesh M_D.

5.2 Two-dimensional case

Consider now the additional constructions required to the implementation of BCAT for the two-dimensional case. We see that the first and the third terms in (3.12) are similar

https://doi.org/10.1017/S0956792598003507 Published online by Cambridge University Press

to (3.13). Therefore, their implementation is done in the same way as for the three-dimensional case – see § 5.1 (naturally, with the use of functions $\{\sin m\phi,\ \cos m\phi\}$ instead of spherical functions).

Extra constructions are necessary only for the second term in (3.12). We approximate the integral in braces by a sum. For this purpose, we make the substitution $s = \alpha \tan\sigma$ where α is a positive number, $\sigma \in [0, \pi/2]$ and introduce a grid $0 = \sigma_0 < \sigma_1 < \cdots < \sigma_{J_q} = \pi/2$ with $\tilde{J}_q$ intervals on the segment $[0, \pi/2]$. Due to the fast decay of $h_{|m|}(r, s)$, see the Lemma in § 3, we use a uniform grid: $\sigma_{j+1} - \sigma_j = \pi/(2\tilde{J}_q)$. Applying the trapezoid rule, we have the following expression for the integral:

$$-\frac{1}{\pi}\int_0^\infty \exp\left(-s(t - \frac{r-R}{c} - t')\right) h_{|m|}(r, s)ds$$

$$\approx \frac{\alpha}{2\tilde{J}_q}\sum_{j=0}^{\tilde{J}_q-1}{}' \exp\left(-s_j(t - \frac{r-R}{c} - t')\right) \frac{h_{|m|}(r, s_j)}{\cos^2(\frac{j\pi}{2\tilde{J}_q})}, \tag{5.3}$$

$$s_j = \alpha \tan\left(\frac{j\pi}{2\tilde{J}_q}\right).$$

Here the prime $(')$ for the sum indicates that the term at $j = 0$ is multiplied by 0.5.

In this procedure, the second term in (3.12) is like the third one, and therefore we can treat it by the same way.

To choose optimal parameters α and $\tilde{J}_q$ in (5.3), we investigated numerically the behaviour of the function

$$\tilde{h}_{|m|}(\sigma) = \frac{h_{|m|}(r, \alpha\tan\sigma)}{\cos^2\sigma}$$

as m varies. It was found that the resolution of the graph of $\tilde{h}_{|m|}(\sigma)$ on a uniform mesh σ_i seems to be best if $\alpha \approx 30$. It was also found that the domain of essential values of $\tilde{h}_{|m|}(\sigma)$ is highly isolated for large m (see Fig. 5); moreover, this domain is narrower and narrower and is moved to the right as $|m|$ increases. Therefore, the contribution of the second term in (3.12) is less and less as $|m| \to \infty$. The most accurate approximation in (5.3) is required only for several small values of $|m| = 0, 1, \ldots$.

In our numerical experiments, it was decided to fix the number of integration points $J_q = 32$ and to make the location of the integration interval depend on m, i.e. to locally refine the integration points. Figures 5 and 6 clarify this rule (left: graph of $\tilde{h}_{|m|}(\sigma) = \frac{h_{|m|}(r, 30\tan\sigma)}{\cos^2\sigma}$, $m = 32$, $r/R = 1.005$, on the whole interval $[0, \pi/2]$; right: close up of this function on the interval of integration (due to a local refinement, the hypothetical value of $\tilde{J}_q$ in (5.3) for this example is estimated as $\tilde{J}_q = 500$)).

5.3 Computational resources required for BCAT on the spherical boundary

Consider first the question of 'how many harmonics should one take to match a given mesh in the computational domain'. Let N be the number of grid intervals around the circle. Take a single harmonic $\exp(iM\phi)$. The approximation error of the second-order difference counterpart to the angular derivative $\partial^2/\partial\phi^2$ in the wave operator for this

https://doi.org/10.1017/S0956792598003507 Published online by Cambridge University Press

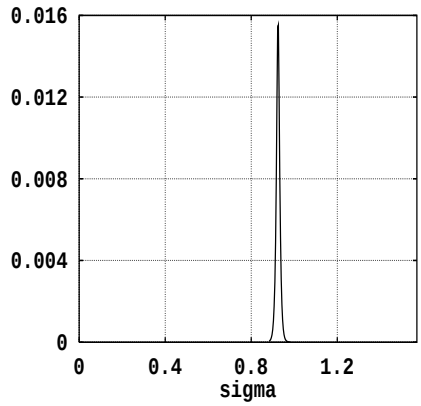

FIGURE 5. Function $\tilde{h}_{32}(\sigma)$, $\sigma \in (0, \pi/2)$.

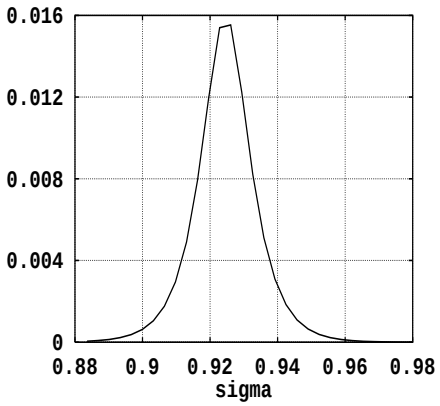

FIGURE 6. Function $\tilde{h}_{32}(\sigma)$ on its interval of integration, number of integration points $J_q = 32$.

function is, evidently, $\mathcal{O}(N^{-2}M^4)$. If we neglect this harmonic in the boundary condition, the error is $\mathcal{O}(1)$. These two errors must correspond to each other, i.e. $const.N^{-2}M^4 \sim 1$. Therefore, we have the estimate $M \sim \sqrt{N}$ for a maximal reasonable value of M. The same estimate $L \sim \sqrt{N}$ is valid for the maximal value of index l in the three-dimensional case when considering the mesh $N \times 2N$ on the sphere.

Two-dimensional case. For each harmonic with the number m we have to calculate: (a) the inner product and the recovering formula (according to Fourier transform); (b) the sum of m terms; and (c) the quadrature sum of J_q terms. Thus the total number of operations at a current time level is estimated as $\mathcal{O}(\sqrt{N}(N + J_q))$. Since we keep $\mathcal{O}(m)$ quantities for each m-th harmonic in the procedure of recurrence calculation with respect to time, the necessary storage is $\mathcal{O}(N + J_q\sqrt{N})$.

Three-dimensional case. The analogous estimates give $\mathcal{O}(N^3)$ for the number of operations, and $\mathcal{O}(N\sqrt{N})$ for the storage.

Assuming that the volume of the grid in the computational domain is $\mathcal{O}(N^2)$ and $\mathcal{O}(N^3)$ for the two- and three-dimensional cases, respectively, we see that BCAT requires negligible computational resources compared with those in the computational domain except for the number of operations in the three-dimensional case.

6 Relation between three-dimensional BCAT and conditions [16]

In this section, we show that conditions proposed in Sofronov [12] and Grote & Keller [16] are equivalent.

Let us fix the index $l > 0$, denote by $u(r, t)$ the corresponding Fourier coefficient $u_l^m(r, t)$, and consider its governing equation:

$$\left[\frac{\partial^2}{\partial t^2} - \frac{\partial^2}{\partial r^2} - \frac{2}{r}\frac{\partial}{\partial r} + \frac{l(l+1)}{r^2}\right] u = 0, \qquad r > 0.$$

https://doi.org/10.1017/S0956792598003507 Published online by Cambridge University Press

In this case, the condition [16] at $r = a$, with $a = 1$ for simplicity, has the form:

$$\left(\frac{\partial}{\partial t} + \frac{\partial}{\partial r}\right)[ru] = f(t) \tag{6.1}$$

where the right-hand side is evaluated by

$$f(t) \equiv -(-1)^l \sum_{j=1}^{l} j\gamma_{lj} w^{(l-j)}(t),$$

$$w^{(l-j)} \equiv \frac{d^{l-j}}{dt^{l-j}} w, \qquad \gamma_{lj} = \frac{(l+j)!}{(l-j)!\,j!\,2^j}, \quad \gamma_{l0} = 1,$$

and function w is the solution of the following Cauchy problem:

$$\left.\begin{aligned} &w^{(l)} + \sum_{j=1}^{l} \gamma_{lj} w^{(l-j)} = (-1)^l u(1,t), \quad t > 0 \\ &w(0) = w^{(1)}(0) = \ldots = w^{(l-1)}(0) = 0. \end{aligned}\right\} \tag{6.2}$$

Let us prove that f can be written out in the explicit form

$$f(t) = \int_0^t E_l^{(3)}(1, t-t')u(1,t')dt'$$

where $E_l^{(3)}$ is from (4.7). Consider the Laplace transform of f. Denote $g(p) = \mathscr{L}[w](p)$. Hence

$$\mathscr{L}[f](p) = -(-1)^l \left[\sum_{j=1}^{l} j\gamma_{lj} p^{l-j}\right] g(p) = -(-1)^l p^{l-1} y_l'(p^{-1}) y_l(p^{-1}) g(p) \tag{6.3}$$

where y_l' is the derivative of the Bessel polynomial

$$y_l(z) = \sum_{j=0}^{l} \gamma_{lj} z^j.$$

Now apply the Laplace transform to (6.2). We have

$$\left[p^l + \sum_{j=1}^{l} j\gamma_{lj} p^{l-j}\right] g(p) = (-1)^l \mathscr{L}[u](p)$$

or

$$p^l y_l(p^{-1}) g(p) = (-1)^l \mathscr{L}[u](p). \tag{6.4}$$

It follows from (6.3), (6.4) that

$$\begin{aligned} \mathscr{L}[f](p) &= -(-1)^l p^{l-1} y_l'(p^{-1})(-1)^l p^{-l} y_l^{-1}(p^{-1}) \mathscr{L}[u](p) \\ &= -p^{-1} y_l'(p^{-1}) y_l^{-1}(p^{-1}) \mathscr{L}[u](p). \end{aligned}$$

Denote by b_j, $j = 1, \ldots, l$, the roots of the Bessel polynomial; hence

$$\mathscr{L}[f](p) = -p^{-1}\left(\sum_{j=1}^{l} \frac{y_l(p^{-1})}{p^{-1} - b_j}\right) y_l^{-1}(p^{-1}) \mathscr{L}[u](p) = \left(\sum_{j=1}^{l} \frac{1}{b_j} \frac{1}{p - \frac{1}{b_j}}\right) \mathscr{L}[u](p).$$

https://doi.org/10.1017/S0956792598003507 Published online by Cambridge University Press

Inverting the Laplace transform, we obtain

$$f(t) = \left(\sum_{j=1}^{l} \frac{1}{b_j} \mathrm{e}^{t/b_j} * \right) u(1,t).$$

The Bessel polynomials are expressed in terms of the Laguerre polynomials $L_l^{(-2l-1)}$, cf. § 3.2, by the following formula:

$$y_l(z) = z^l \frac{(2l)!}{l!2^l} L_l^{(-2l-1)}(2/z).$$

Therefore $b_j = 2/z_j^l$. Thus we see that the non-local terms in boundary conditions (4.6) at $c = 1$ and (6.1) are the same, i.e. the conditions are equivalent.

7 Numerical examples

7.1 Tests for separate Fourier harmonics

To validate the formulae described in Stage 2 of § 5.1, we consider the following set of one-dimensional initial boundary-value problems for the coefficients v at spherical harmonics Y_l^m with different values $l = 0, 1, \ldots$:

$$\begin{array}{lll} \dfrac{\partial^2 v}{\partial t^2} - \dfrac{1}{r}\dfrac{\partial^2 (rv)}{\partial r^2} + \dfrac{l(l+1)}{r^2} v = 0, & r > a, & t > 0 \\ v|_{t=+0} = \omega(r), & r > a & \\ \frac{\partial v}{\partial t}|_{t=+0} = 0, & r > a & \\ v|_{r=a} = 0, & & t > 0, \end{array}$$

where $\omega(r)$ is an initial function of 'cap' type:

$$\omega(r) = \begin{cases} \exp\left(\frac{-4(r-(a+b)/2)^2}{(b-a)^2/4-(r-(a+b)/2)^2} \right), & a < r < b \\ 0, & r \geqslant b \end{cases}.$$

This problem is approximated by a difference one with a central-difference leap-frog scheme on the mesh

$$\begin{array}{llll} r_i = a + ih, & i = 0, 1, \cdots, & h = (1-a)/I, & a = 0.25, b = 0.75 \\ t_n = n\tau, & n = 0, 1, \cdots, & \tau = Ch, & C = 0.5. \end{array}$$

To check the accuracy of the difference counterpart to BCAT, two initial boundary value problems are considered simultaneously for each parameters l and I: the problem on the interval $a < r < 1$ with BCAT at $r = 1$; and the problem on the semi-axis $r > a$ without any boundary condition at the right or, in other words, with the Free Condition (FC). Both solutions, S_{BCAT} and S_{FC}, are calculated till the time $t = 2$. Figure 7 shows the solutions and the difference between them at the intermediate time $t = 1$; here the parameter $l = 3$.

Denote $\varepsilon = \max_{t \in (0,2)} |S_{FC} - S_{BCAT}|$ at $r = 1$. Table 1 shows the values of $\log_4 \varepsilon$ for different variants.

We see distinctly the quadratic decay of the error ε for the generated difference counterpart of BCAT.

https://doi.org/10.1017/S0956792598003507 Published online by Cambridge University Press

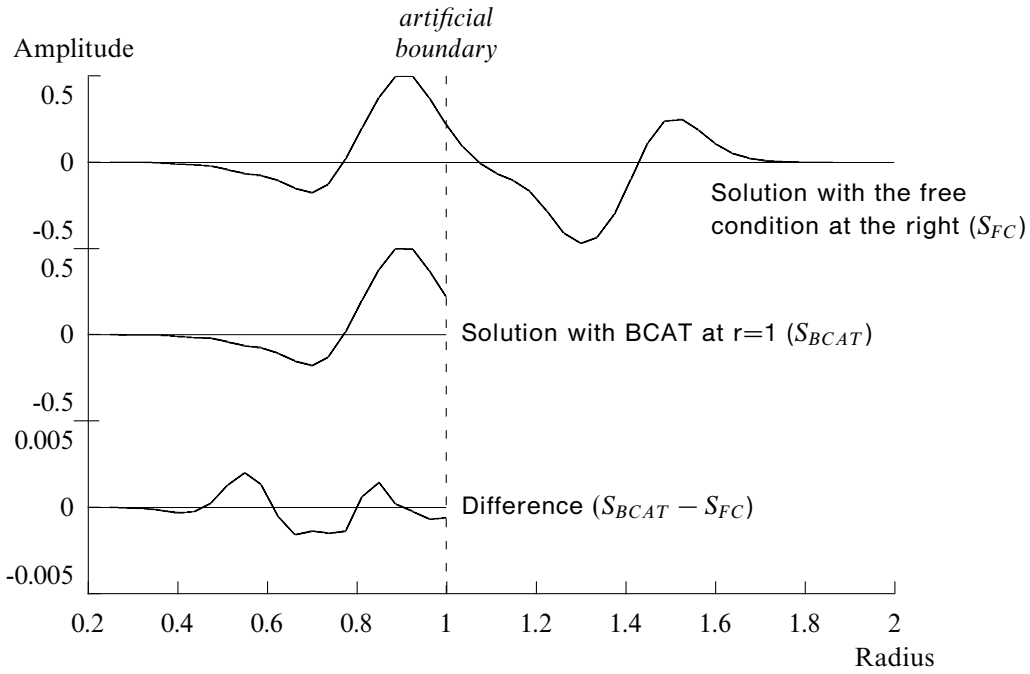

FIGURE 7. Amplitudes of solutions and difference between them at $t = 1$ (variant with parameters $l = 3, I = 20$).

Table 1. *Three-dimensional case, value of* $\log_4 \varepsilon$.

	$l = 1$	$l = 2$	$l = 3$	$l = 6$
I=20	−4.35	−4.23	−4.16	−4.01
I=40	−5.53	−5.56	−5.52	−5.34
I=80	−6.66	−6.57	−6.54	−6.40
I=160	−7.64	−7.56	−7.53	−7.40

The same test was done for the two-dimensional wave equation. The only difference was in the construction of BCAT and in the governing equation for v:

$$\frac{\partial^2 v}{\partial t^2} - \frac{1}{r}\frac{\partial}{\partial r}\left(r\frac{\partial v}{\partial r}\right) + \frac{m^2}{r^2}v = 0.$$

Figure 8 shows the values of $\log_4 \varepsilon$ versus m for different grid parameters I. At each fixed m the error ε decays quadratically while doubling I. The parameter J_q (see § 5.2) was $J_q = 32$ for all the calculations.

To check the numerical stability of BCAT for a long time, the calculations for several numbers of l and m were continued till time $t = 20$. No problems with stability were observed.

https://doi.org/10.1017/S0956792598003507 Published online by Cambridge University Press

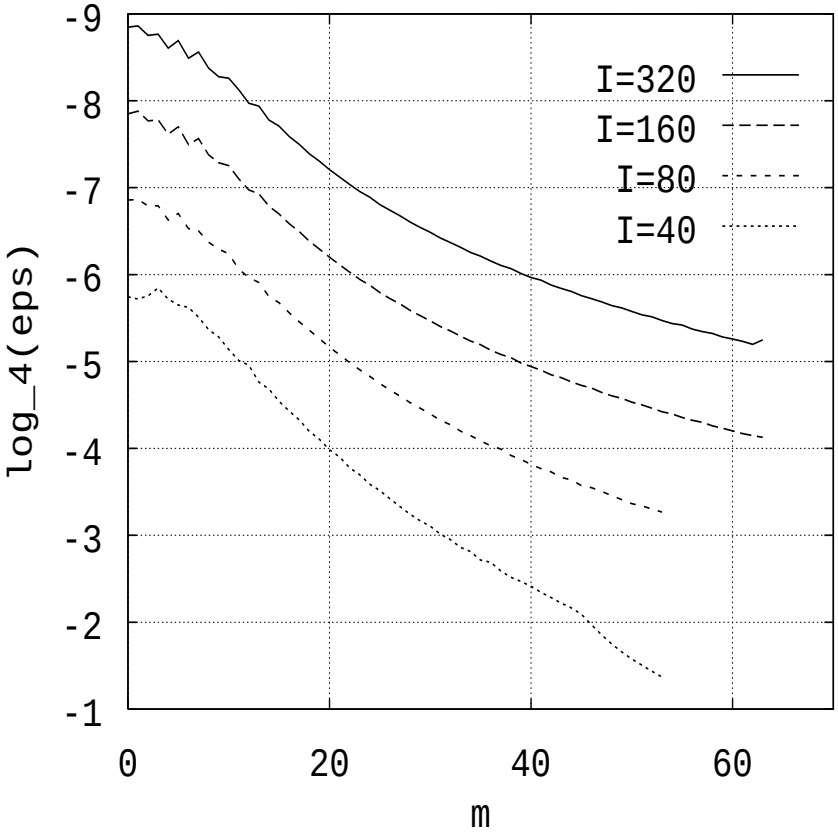

FIGURE 8. Error $\varepsilon = \max_{t\in(0,2)}|S_{FC} - S_{BCAT}|$ versus $|m|$ for grids with $I = 40, 80, 160, 320$.

7.2 Test examples in three-dimensions

We check the properties of BCAT for three-dimensional problems on the same test examples that are used by Grote & Keller [17]. The following geometry is considered (see Fig. 9): S is the scattering sphere, $r_S = 0.5$; $B\backslash S$ is the computational domain, $r_B = 1$; G is the ball with a non-zero source g in the wave equation $u_{tt} - \Delta u = g$, $r_G = 0.15$, the centre $\mathbf{x}_G$ of G is at $r = 0.75$, $\theta = 0$.

The function g has the form

$$g(\mathbf{x}, t) = \begin{cases} \beta \sin(\omega t)\sin^2(1 - |\mathbf{x} - \mathbf{x}_G|/r_G)\pi/2, & \text{if } x \in G \\ 0, & \text{otherwise.} \end{cases}$$

The initial data are homogeneous: $u = u_t = 0$ at $t = 0$.

We use the spherical system of coordinates (r, θ, ϕ) to solve this problem numerically. Since the solution does not depend on ϕ, the coordinates (r, θ) are only considered. We introduce a uniform spherical mesh shifted from the poles:

$$r_i = r_S + ih_r, \quad h_r = (r_B - r_S)/I, \quad i = 0, 1, ..., I;$$

$$\theta_j = (j + \tfrac{1}{2})h_\theta, \quad h_\theta = \pi/J, \quad j = 0, 1, ..., J - 1;$$

https://doi.org/10.1017/S0956792598003507 Published online by Cambridge University Press

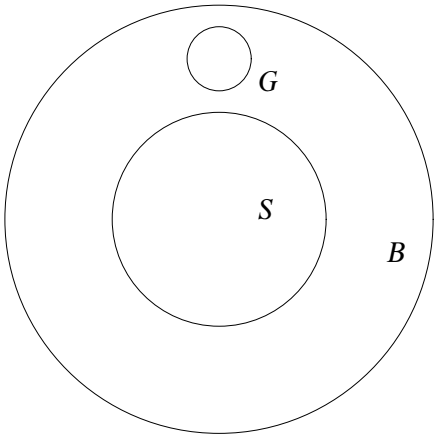

FIGURE 9. Computational domain $B\backslash S$ and source domain G.

and discretize the wave equation in the following way:

$$\frac{u_{i,j}^{n+1}-2u_{i,j}^{n}+u_{i,j}^{n-1}}{\tau^2}-\frac{1}{r_i^2}\frac{r_{i+0.5}^2(u_{i+1,j}^{n}-u_{i,j}^{n})-r_{i-0.5}^2(u_{i,j}^{n}-u_{i-1,j}^{n})}{h_r^2}$$

$$-\frac{1}{r_i^2}\frac{1}{\sin\theta_j}\frac{\sin\theta_{j+0.5}(u_{i,j+1}^{n}-u_{i,j}^{n})-\sin\theta_{j-0.5}(u_{i,j}^{n}-u_{i,j-1}^{n})}{h_\theta^2}=g(t_n,r_i,\theta_j)$$

where $n=1,2,\ldots$; $i=1,\ldots,I-1$; $j=1,\ldots,J-1$; $r_{i\pm0.5}=r_i\pm0.5h_r$; $\theta_{j\pm0.5}=\theta_j\pm0.5h_\theta$; $u_{i,j}^n\equiv u(t_n,r_i,\theta_j)$.

The boundary condition at the scatterer is $u_{1,j}^n-u_{0,j}^n=0$; the initial conditions are $u_{i,j}^0=u_{i,j}^1=0$.

At $r_I=r_B$ we impose our BCAT that must provide transparency of the boundary ∂B for outgoing waves. The procedure is following. Let L be a maximal value of index l in the calculation formulae for discrete BCAT – see § 5.1 (here $\mathscr{M}=\{0,1,\ldots,L\}$). Denote by $[u_{I-1}^n]_L$ the projection of a discrete function u_{I-1}^n onto subspace of *DSFs* with indexes from $\mathscr{M}$. We apply BCAT for $[u_{I-1}^n]_L$, and calculate the function $[u_I^{n+1}]_L$. For a 'non-smooth' remainder part $v_I^n=u_I^n-[u_I^n]_L$ we apply a discrete counterpart of the commonly used boundary condition

$$v_t+v_r+\frac{1}{r}v=0 \tag{7.1}$$

and obtain the function v_I^{n+1}. The result function $u_I^{n+1}=[u_I^{n+1}]_L+v_I^{n+1}$. We shall denote such condition by BCAT(L). Note that it corresponds to the condition *NR1(L)* introduced by Grote & Keller [17]. Clearly, BCAT(0) coincides with (7.1).

To compare our solution with the solution of the problem in the infinite domain $\mathbb{R}^3\backslash S$, we extend the mesh up to $r=5$ and solve the problem for this large domain as well. The solution in the large domain gives us the 'exact' solution in the computational domain $B\backslash S$ up to the time level $t=8$ (after this moment, the reflections from the external boundary $r=5$ reach the ball B).

https://doi.org/10.1017/S0956792598003507 Published online by Cambridge University Press

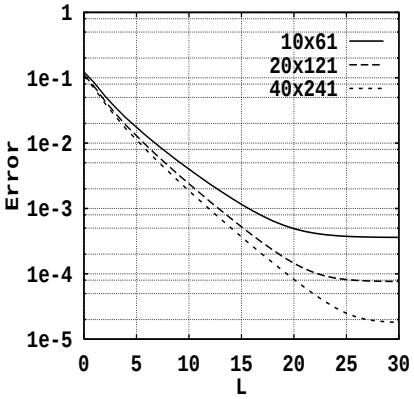

FIGURE 10. Three-dimensional case. Error ε_L for different grids, $\omega = 0.25$.

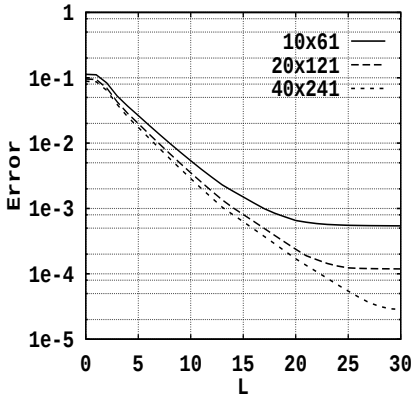

FIGURE 11. Three-dimensional case. Error ε_L for different grids, $\omega = 1$.

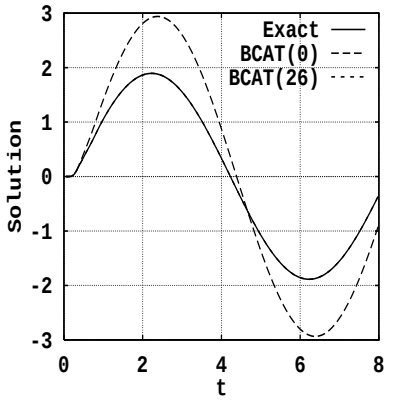

FIGURE 12. Three-dimensional case. Solutions $u_{ex}(t)$, $u_0(t)$, $u_{26}(t)$ at $r = 1, \theta = 0$; grid 20×121; $\omega = 0.25$.

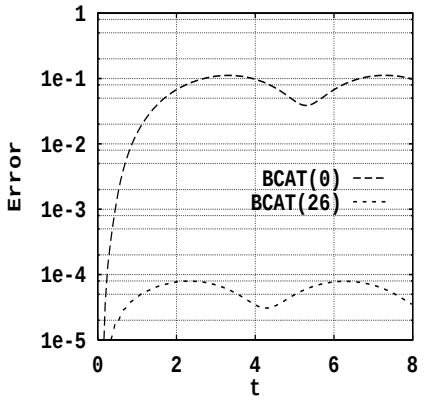

FIGURE 13. Three-dimensional case. Errors $\varepsilon_0(t), \varepsilon_{26}(t)$; grid 20×121; $\omega = 0.25$.

Denote by

$$\varepsilon_L(t) = \|u_{ex}(t) - u_L(t)\|_{L_2(B\setminus S)} \tag{7.2}$$

the L_2-error between exact solution u_{ex} and solution u_L with BCAT(L). Introduce also

$$\varepsilon_L = \max_{t\in(0,8)} \varepsilon_L(t).$$

Figures 10 and 11 show the maximal error ε_L versus L for three meshes $I \times J$ (left: for $\omega = 0.25$ in the source function; right: for $\omega = 1$). We see that for each mesh size, the error decreases if the number L increases till some fixed value. Therefore, we find that the accuracy of the discrete counterpart of BCAT corresponds to the accuracy of the difference scheme near $L = 23,\ 25,\ 29$ for grids $10 \times 61,\ 20 \times 121,\ 40 \times 241$, respectively. Due to applying the BCAT instead of condition (7.1), the accuracy of the calculations increases for considered grids 300, 1400, 5800 times, respectively (for $\omega = 0.25$).

Figure 12 shows the behaviour of solutions for $\omega = 0.25$ at the point $r = 1, \theta = 0$; grid is $20 \times 121,\ \beta = 2000$. The exact solution and the solution with condition (7.1) (BCAT(0))

https://doi.org/10.1017/S0956792598003507 Published online by Cambridge University Press

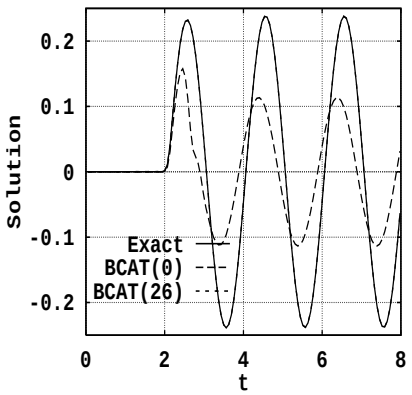

FIGURE 14. Three-dimensional case. Solutions $u_{ex}(t)$, $u_0(t)$, $u_{26}(t)$ at $r = 1, \theta = \pi$; grid 20×121; $\omega = 1$.

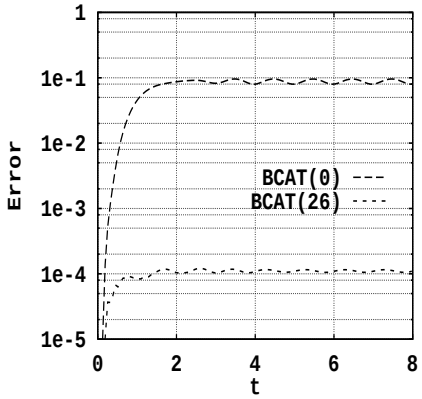

FIGURE 15. Three-dimensional case. Errors $\varepsilon_0(t), \varepsilon_{26}(t)$; grid 20×121; $\omega = 1$.

differ essentially from each other. At the same time, the difference between the exact solution and the solution with BCAT(26) cannot be distinguished on the graph. Figure 13 gives the value of $\varepsilon_L(t)$ versus t. The results corresponding to $\omega = 1$ at the observation point $r = 1,\ \theta = \pi$ are shown in Figures 14 and 15.

7.3 Test examples in two-dimensions

The first test has the same setup as for the three-dimensional case, i.e. θ is now the polar angle and we denote it by ϕ; parameter $\beta = 200$ for the source g. Due to the symmetry, we consider the problem in the half-plane $x \geqslant 0$, i.e. $|\phi| \leqslant \pi/2$. The mesh for the variable ϕ is

$$\phi_j = \pi/2 - jh_\phi, \quad h_\phi = \pi/J, \quad j = 0, ..., J,$$

and the wave equation is discretized by

$$\frac{u^{n+1}_{i,j} - 2u^n_{i,j} + u^{n-1}_{i,j}}{\tau^2} - \frac{1}{r_i}\frac{r_{i+0.5}(u^n_{i+1,j} - u^n_{i,j}) - r_{i-0.5}(u^n_{i,j} - u^n_{i-1,j})}{h_r^2}$$

$$-\frac{1}{r_i^2}\frac{u^n_{i,j+1} - 2u^n_{i,j} + u^n_{i,j-1}}{h_\phi^2} = g(t_n, r_i, \phi_j).$$

Again our discrete artificial boundary condition BCAT(M) consists of a 'smooth' part that treats a fixed number M of Fourier coefficients according to formulae of § 5.2, and a 'non-smooth' part that treats the remainder by the known condition

$$v_t + v_r + \frac{1}{2r}v = 0 \tag{7.3}$$

For convenience, we will denote the condition (7.3) by BC0 and the corresponding error in (7.2) by ε_0. Note that (7.3) does not coincide with BCAT(0), i.e. with condition (4.5) when $m = 0$.

Figures 16–21 show the results of the two-dimensional calculations that correspond to

https://doi.org/10.1017/S0956792598003507 Published online by Cambridge University Press

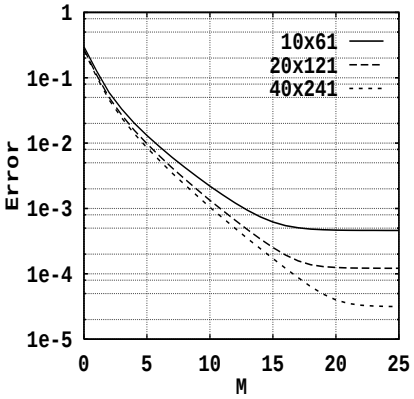

FIGURE 16. Two-dimensional case. Error ε_M for different grids, $\omega = 0.25$.

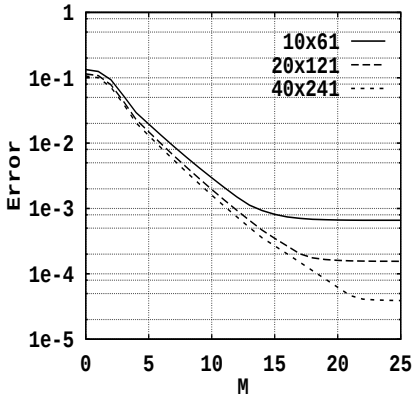

FIGURE 17. Two-dimensional case. Error ε_M for different grids, $\omega = 1$.

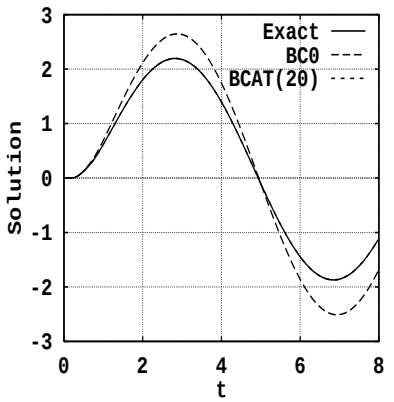

FIGURE 18. Two-dimensional case. Solutions $u_{ex}(t)$, $u_0(t)$, $u_{20}(t)$ at $r = 1, \phi = \pi/2$; grid 20×121; $\omega = 0.25$.

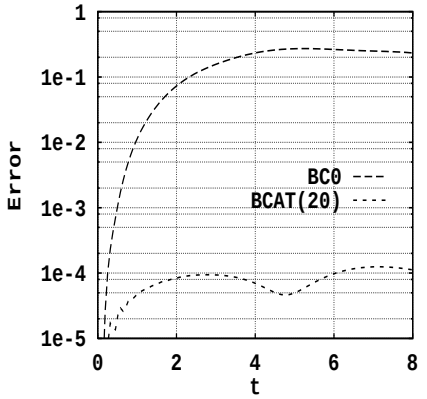

FIGURE 19. Two-dimensional case. Errors $\varepsilon_0(t), \varepsilon_{20}(t)$; grid 20×121; $\omega = 0.25$.

the three-dimensional test problem formulations described in the previous item. Here the optimal values of M are 17, 19, 22 for grids 10×61, 20×121, 40×241, respectively.

The second test example corresponds to one of the benchmarks from [24]. The scatterer is the circle $r_S = 0.5$. The unknown function v (pressure) satisfies the two-dimensional wave equation and has the following initial condition at $t = 0$:

$$v = 2^{-\frac{(x-4)^2+y^2}{0.04}}.$$

To calculate the solution, we close the computational domain by a circular artificial boundary with $r_B = 5$ and use a uniform polar mesh 180×500, so $h_r = 4.5/180$, $h_\phi = \pi/500$, $\tau = 0.0015$. The 'exact' solution until $t = 10$ for $r \leqslant 5$ is calculated by using a larger domain with the external circular boundary $r = 10$. Figure 22 shows $v(t)$ at $r = 5$, $\phi = \pi/2$ for different parameters M in BCAT(M). The graph of solution with BCAT(63) coincides practically with the graph of the exact solution. Figure 23 shows the L_2-error $\varepsilon_M(t)$ defined by (7.2). The fragment of the solution along the segment $0.5 \leqslant r \leqslant 5$, $\phi = \pi/2$ at $t = 7$ is

https://doi.org/10.1017/S0956792598003507 Published online by Cambridge University Press

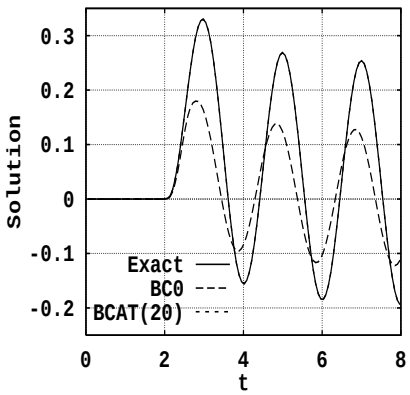

FIGURE 20. Two-dimensional case. Solutions $u_{ex}(t)$, $u_0(t)$, $u_{20}(t)$ at $r = 1, \phi = -\pi/2$; grid 20×121; $\omega = 1$.

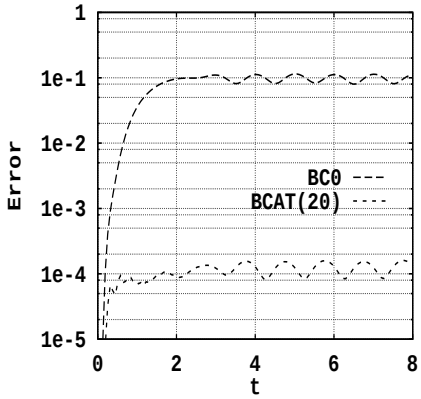

FIGURE 21. Two-dimensional case. Errors $\varepsilon_0(t), \varepsilon_{20}(t)$; grid 20×121; $\omega = 1.0$.

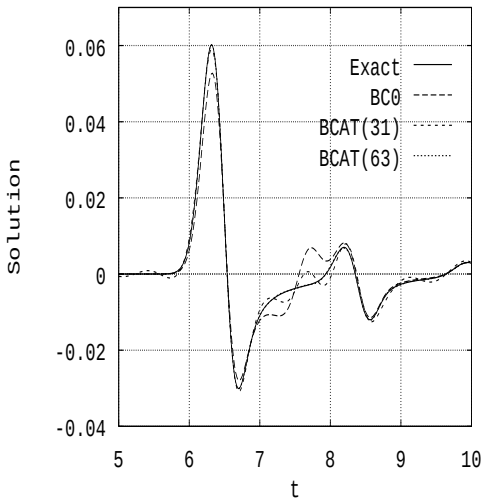

FIGURE 22. Exact solution and solution with condition (7.3), BCAT(31), and BCAT(63) versus t at the point $r = 5$, $\phi = \pi/2$.

given in Fig. 24; we can see that only in the vicinity of $r = 4.4$ is the difference between the exact solution and the solution with BCAT(63) visible.

8 Conclusion

Exact artificial boundary conditions, BCAT, for both two- and three-dimensional wave equation are described. The conditions permit us to reduce free-space scattering problems to problems in finite (truncated) domains. The corresponding operators have an explicit form with a non-local part consisting of the Fourier transform with respect to space variables and convolutions with respect to time.

An efficient numerical implementation of BCAT is proposed. The method permits us to

https://doi.org/10.1017/S0956792598003507 Published online by Cambridge University Press

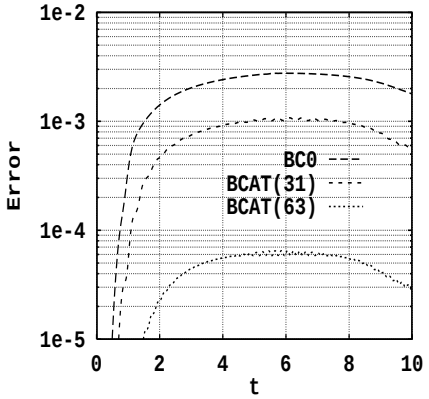

FIGURE 23. Errors $\varepsilon_0(t), \varepsilon_{31}(t), \varepsilon_{63}(t)$.

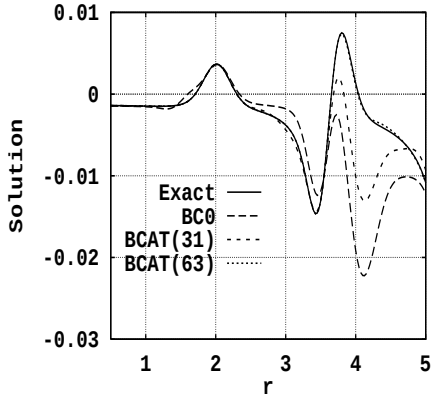

FIGURE 24. Exact solution and solutions with conditions (7.3), BCAT(31), and BCAT(63) versus r at $\phi = \pi/2,\ t = 7$.

evaluate the convolution integrals by recurrence formulae with respect to time. As a result, additional computational costs on the boundary of a domain, which are required while using BCAT, are at least not greater than that inside the domain. Besides, the method treats the general case of non-spherical meshes.

The equivalence of BCAT in three space dimensions and the nonreflecting boundary conditions [16] is proved. It is worth noting that, unlike the condition [16], the numerical implementation of BCAT covers two space dimensions and non-spherical computational domains.

The calculation of test scattering problems presented above and in [17] demonstrate the high superiority of exact ABCs based on the Fourier method for spherical and polar grids. The numerical investigation of our conditions coupled with a Cartesian mesh in the computational domain is planned.

Acknowledgement

This research was supported by the Alexander von Humboldt Foundation while the author was visiting Stuttgart University.

Appendix

We give here the calculation of the limit used for deriving $E_m^{(2)}(r,t)$.

$$\lim_{\varepsilon\to 0}\frac{1}{\varepsilon}h_{|m|}(R+\varepsilon,s) = \lim_{\varepsilon\to 0}\frac{1}{\varepsilon}\mathrm{Im}\frac{\Psi(|m|+\frac{1}{2},2|m|+1;-s+\frac{\varepsilon}{R}s+i0)}{\Psi(|m|+\frac{1}{2},2|m|+1;-s+i0)}$$

$$= \lim_{\varepsilon\to 0}\frac{1}{\varepsilon}\mathrm{e}^{-\frac{\varepsilon}{R}s}\mathrm{Im}\frac{C_m\Phi(*;s+\frac{\varepsilon}{R}s)i+\Psi(*;s+\frac{\varepsilon}{R}s)}{C_m\Phi(*;s)i+\Psi(*;s)}$$

$$= \lim_{\varepsilon\to 0}\frac{1}{\varepsilon}\mathrm{e}^{-\frac{\varepsilon}{R}s}C_m\frac{\Phi(*;s+\frac{\varepsilon}{R}s)\Psi(*;s)-\Psi(*;s+\frac{\varepsilon}{R}s)\Phi(*;s)}{C_m^2\Phi^2(*;s)+\Psi^2(*;s)}$$

https://doi.org/10.1017/S0956792598003507 Published online by Cambridge University Press

$$= C_m \frac{s}{R} \frac{\Phi'(*;s)\Psi(*;s) - \Psi'(*;s)\Phi(*;s)}{C_m^2\Phi^2(*;s) + \Psi^2(*;s)}$$

$$= C_m \frac{s}{R} \frac{\Gamma(2|m|+1)}{\Gamma(|m|+\frac{1}{2})} \frac{\mathrm{e}^s s^{-(2|m|+1)}}{C_m^2\Phi^2(*;s) + \Psi^2(*;s)}$$

$$= (-1)^{|m|+1}\mathrm{e}^s \frac{s^{-2|m|}}{R} \frac{1}{s^{-2|m|}\mathrm{e}^s\left[\pi\,\mathrm{I}_m^2(s/2) + \frac{1}{\pi}\mathrm{K}_m^2(s/2)\right]}$$

$$= (-1)^{|m|+1}\frac{1}{R}\frac{\pi}{\pi^2\,\mathrm{I}_m^2(s/2) + \mathrm{K}_m^2(s/2)}.$$

Here $C_m = \frac{\sqrt{\pi}(-1)^{|m|+1}}{4^{|m|}|m|!}$, $\Gamma(x)$ is the Gamma-function. To simplify the formulae, the asterisk '$*$' is used instead of the combination of symbols '$|m|+\frac{1}{2}, 2|m|+1$'.

References

[1] Engquist, B. & Majda, A. (1977) Absorbing boundary conditions for the numerical simulation of waves. *Math. Comput.* **31**, 629–651.

[2] Higdon, R. L. (1986) Absorbing boundary conditions for difference approximations to the multidimensional wave equation. *Math. Comput.* **47**, 437–459.

[3] Blaschak, J. G. & Kriegsmann, G. A. (1988) A comparative study of absorbing boundary conditions. *J. Comput. Phys.* **77**, 109–139.

[4] Bayliss, A. & Turkel, E. (1980) Radiation boundary conditions for wave-like equations. *Commun. Pure Appl. Math.* **XXXIII**, 707–725.

[5] Hagstrom, T. M. (1991) Asymptotic boundary conditions for dissipative waves: general theory. *Math. Comput.* **56**, 589–606.

[6] Berenger, J.-P. (1994) A perfectly matched layer for absorption of electromagnetic waves. *J. Comput. Phys.* **114**, 185–200.

[7] Givoli, D. (1991) Non-reflecting boundary conditions. *J. Comp. Phys.* **94**, 1–29.

[8] Tsynkov, S. V. (1998) Numerical solution of problems on unbounded domains: A review. *Appl. Numer. Math.* (to appear).

[9] Ting, L. & Miksis, M. J. (1986) Exact boundary conditions for scattering problems. *J. Acoust. Soc. Am.* **80**, 1825–1827.

[10] Givoli, D. & Gohen, D. (1995) Nonreflecting boundary conditions based on Kirchhoff-type formulae. *J. Comp. Phys.* **117**, 102–113.

[11] Lyrintzis, A. S. (1994) Review: The Use of Kirchhoff's method in computational aeroacoustics. *J. Fluids Eng.* **116**(12), 665–676.

[12] Sofronov, I. L. (1993) Conditions for complete transparency on the sphere for the three-dimensional wave equation. *Russian Acad. Sci. Dokl. Math.* **46**, 397–401.

[13] Sofronov, I. L. (1993) Condition of absolute transparency on sphere for wave equation. In: K. Morgan, E. Oñate, J. Periaux, J. Peraire and O. C. Zienkiewicz (eds.), *Finite Elements in Fluids; New Trends and Applications*, pp. 1387–1396. CIMNE, Barcelona, Pineridge Press, Spain.

[14] Sofronov, I. L. (1993) *Condition of absolute transparency for the wave equation.* Preprint No. 76, Keldysh Institute of Applied Mathematics, Rus. Acad. Scis. (in Russian).

[15] Sofronov, I. L. (1996) *Generation of 2D and 3D artificial boundary conditions transparent for waves outgoing to infinity*. Preprint 96-09 of Mathematical Institute A, Stuttgart University.

[16] Grote, M. J. & Keller, J. B. (1995) Exact nonreflecting boundary conditions for the time dependent wave equation. *SIAM J. Appl. Math.* **55**(2), 280–297.

https://doi.org/10.1017/S0956792598003507 Published online by Cambridge University Press

[17] Grote, M. J. & Keller, J. B. (1996) Nonreflecting boundary conditions for time-dependent scattering. *J. Comp. Phys.* **127**, 52–65.
[18] Ryaben'kii, V. S. (1990) Exact transfer of difference boundary conditions. *Functional Anal. Appl.* **24**, 251–253.
[19] Ryaben'kii, V. S. (1990) Exact transfer of boundary conditions. *Computational Mechanics of Solids* **1**, 129–145 (in Russian).
[20] George, A. R. & Lyrintzis, A. S. (1988) Acoustics of transonic blade-vortex interactions. *AIAA J.* **26**(7), 769–776.
[21] Körber, S. & Ballmann, J. (1995) Mechanisms and acoustics of blade-vortex-interactions. *Z. Flugwiss. Weltraumforsch.* **19**, 397–406.
[22] Sofronov, I. L. (1995) *Transparent boundary conditions for unsteady transonic flow problems in wind tunnel.* Preprint 95-21 of Mathematical Institute A, Stuttgart University.
[23] Sofronov, I. L. (1998) Non-reflecting inflow and outflow in wind tunnel for transonic time-accurate simulation. *J. Math. Anal. Appl.* **221**, 92–115.
[24] *Second Computational Aeroacoustics Workshop on Benchmark Problems* (4–5 November 1996) Florida State University, Tallahassee, FL.
[25] Ditkin, V. A. & Prudnikov, A. P. (1974) *Integral Transforms and Operational Calculus.* Moscow, Nauka (in Russian).
[26] Erdélyi, A. (1953) *Higher transcendental functions. Vol. 1 (Bateman Project).* New-York, McGraw–Hill.
[27] Watson, G. N. (1944) *A treatise on the theory of Bessel functions.* Cambridge, 1944.
[28] Ryaben'kii, V. S. & Sofronov, I. L. (1983) *Difference spherical functions.* Preprint No. 75, Keldysh Institute of Applied Mathematics, USSR Academy of Sciences (in Russian).
[29] Ryaben'kii, V. S. (1987) *Difference potentials method for some problems of continuous media mechanics.* Moscow, Nauka (in Russian).